Global Academic and Scientific Journal of Multidisciplinary Studies (GASJMS)

Volume 4 | Issue 6, 2026 Homepage: https://gaspublishers.com/gasjms/ ISSN: 2583-8970

Ecological Risk and Mobility Assessment of Heavy Metals in Soils from the Ikole–Itapaji Area, Southwestern Nigeria

Adeleke Ojo, Olusola Amos Olaolorun and Adeyinka Aturamu

ORCID: 0009-0000-3106-2704

Department of Geology/Applied Geophysics, Ekiti State University, Ado Ekiti

Received: *11.05.2026* | ***Accepted:*** *13.06.2026* | ***Published:*** *17.06.2026*

***Corresponding Author:** Adeleke Ojo

DOI: *10.5281/zenodo.20727426*

Abstract **Original Research Article**

This study evaluates the ecological risk and mobility behavior of heavy metals in soils from the Ikole–Itapaji area, Southwestern Nigeria, using the Ecological Risk Index (ERI) and Mobility Factor (MF) within a multi-fraction geochemical framework. The study area lies within the Precambrian Basement Complex of the West African Craton, characterized by migmatite–gneiss, granitic, and schistose lithologies that influence the natural geochemical background of soils. Surface soil samples collected from seventeen locations were subjected to a seven-step sequential extraction procedure to determine metal partitioning across water-soluble, exchangeable, carbonate-bound, Fe–Mn oxide-bound, organic-bound, sulfide/strongly bound, and residual phases. The Ecological Risk Index results indicate spatial variability in contamination levels, with SQ4 and SQ15 exhibiting very high ecological risk (ERI = 629.72 and 655.88, respectively), while most other locations fall within moderate to considerable risk categories. The Mobility Factor results reveal generally low mobility across the study area (2.7%–4.0%), indicating that most heavy metals are predominantly associated with stable geochemical phases. However, slightly elevated mobility at SQ4 and SQ15 suggests localized enhancement of metal reactivity and potential bioavailability. Integrated interpretation shows a strong coupling between ecological risk and metal mobility, with cadmium identified as the primary contaminant driving both enrichment and ecological hazard. The combined ERI and MF approach confirms that while the Basement Complex geology exerts a dominant control on metal stabilization, localized anthropogenic inputs contribute to elevated contamination and environmental risk in specific hotspot areas. The study highlights the need for targeted environmental monitoring and sustainable land-use management in the identified high-risk zones

Keywords: Ecological Risk Index, Mobility Factor, Heavy metals, Sequential extraction, Basement Complex, Ikole–Itapaji

1.0 INTRODUCTION

Heavy metals are naturally present in soils as components of parent rock materials; however, their concentrations may be significantly modified by both natural geochemical processes and anthropogenic activities such as agriculture, urbanization, and small-scale mining. Due to their

persistence, toxicity, and non-biodegradable nature, the accumulation of heavy metals in soils has become a major environmental concern, particularly with respect to ecosystem stability and human health risks (Firmino et al., 2025).

Total metal concentration alone is insufficient for evaluating environmental impact, as it does not account for toxicity, ecological sensitivity, or bioavailability. Consequently, the Ecological Risk Index (ERI) has been widely applied as a risk-based approach for assessing the potential ecological threat posed by heavy metals. ERI integrates metal concentration, toxicity response factors, and background reference values to provide a quantitative measure of ecological risk, allowing classification of contamination levels from low to very high risk depending on metal toxicity and abundance (Firmino et al., 2025).

In addition, the Mobility Factor (MF) is an important geochemical indicator used to evaluate the mobility and potential bioavailability of heavy metals in soils. It is commonly derived from sequential extraction data and represents the proportion of metals present in the more labile fractions such as water-soluble, exchangeable, and carbonate-bound phases. High MF values indicate greater potential for leaching, plant uptake, and ecological exposure, whereas low values suggest that metals are predominantly bound to stable mineral phases and are less environmentally available (De Matteis et al., 2023; Ibrahim et al., 2024). Sequential extraction techniques, such as the Tessier and BCR procedures, further provide a framework for understanding metal speciation and environmental behavior in soil systems (Ibrahim et al., 2024). Metals associated with non-residual fractions are generally considered more mobile and potentially anthropogenic, while those in residual fractions are typically lithogenic in origin and structurally bound within mineral lattices (Firmino et al., 2025). Processes such as adsorption onto Fe–Mn oxides and association with organic matter also play key roles in controlling metal redistribution and mobility in soils (Delina, 2024).

The Ikole–Itapaji area of Southwestern Nigeria is underlain by Precambrian Basement Complex rocks, including migmatite–gneiss, charnockite, and granitic lithologies, which strongly influence the natural geochemical background of soils in the region. Despite its geological significance, limited studies have focused on the ecological risk and mobility behavior of heavy metals in surface soils, leaving a gap in understanding their environmental implications and geochemical controls.

Therefore, this study integrates the Ecological Risk Index (ERI) and Mobility Factor (MF) to assess the ecological risk status, mobility characteristics, and potential environmental behavior of selected heavy metals in soils from the Ikole–Itapaji area, Southwestern Nigeria. The study further aims to improve understanding of contamination severity, metal mobility, and associated ecological implications within this Basement Complex terrain (Firmino et al., 2025; Çelebi, 2024; Abule and Ekpete, 2025).

2.0 Description of study area

The study area is located within the Ikole–Itapaji axis of Ekiti State in Southwestern Nigeria, forming part of the Precambrian Basement Complex of the West African Craton. It lies approximately between latitudes 7°45′N–8°05′N and longitudes 5°20′E–5°40′E, covering an estimated total surface area of approximately 1,360 km². encompassing Ikole-Ekiti, Itapaji, and adjoining settlements. The terrain is characterized by undulating topography with elevations ranging from about 300 to over 600 m above sea level, typical of basement terrains marked by ridges and inselbergs (Ojo et al., 2024). Geologically, the area is dominated by migmatite–gneiss complexes, granitic intrusions, and minor schist belts, which are characteristic of the Nigerian Basement Complex and are widely associated with mineralization processes (Adetunla et al., 2025). These lithologies have undergone multiple episodes of deformation, metamorphism, and magmatism, resulting in well-developed structural features, including faults, fractures, and joints, which serve as conduits for hydrothermal fluids (Ogah & Abubakar, 2024). The occurrence of pegmatitic intrusions within the granitic units further enhances the area's mineralization potential, particularly for rare metals.

Climatically, the region falls within the tropical humid zone, with distinct wet and dry seasons and

annual rainfall exceeding 1200 mm. Vegetation is mainly derived from a savannah with patches of secondary forest, which moderately affects surface exposure during geological and remote sensing investigations. The area is relatively accessible through a network of roads linking Ikole-Ekiti to other parts of Ekiti State. Overall, the favourable lithological composition, combined with a complex structural framework, makes the Ikole–Itapaji area a promising target for integrated geophysical and remote sensing studies to delineate zones of mineralization (Salako et al., 2024).

2.1 Field description of the study area

Table 1 presents the field descriptions and geographic coordinates of seventeen **(17)** soil samples collected from different locations within the Ikole–Itapaji area of Southwestern Nigeria. The sampling points are spatially distributed across several settlements and farmland environments including Igbona-Ile, Agbeyewa Farm, Aba Farm, Esun, Omu, Iyemero, Odo-Oro, and Itapaji, thereby ensuring adequate representation of the study area. The geographic coordinates indicate that the sampled locations fall within latitudes 7°45′N to 7°59′N and longitudes 5°26′E to 5°33′E, reflecting a wide spatial coverage across the basement complex terrain. Elevation values vary considerably from 447 m to 588 m above sea level, suggesting moderate topographic variation within the study area, which may influence weathering intensity, drainage conditions, and elemental redistribution in the soils.

The sampled soils were collected at shallow depths ranging from 0.25 m to 0.60 m, representing near-surface regolith materials that are more susceptible to anthropogenic influence, weathering processes, and metal mobility. Field descriptions reveal considerable lithological and textural variability, with the soils comprising laterite, sandy clay, lateritic sand, gravelly sand, clayey sand, sandy loam, gravelly clay, and sand. Lateritic and reddish-brown soils dominate several locations such as SQ1, SQ6, SQ8, and SQ15, indicating intense tropical weathering and iron oxide enrichment typical of Precambrian Basement Complex terrains. Brown to dark brown soil colours observed in many locations suggest varying proportions of organic matter, clay minerals, and iron-bearing constituents. The occurrence of gravelly and sandy materials in some sampling points further indicates active mechanical weathering and sediment reworking processes. Overall, the field characteristics demonstrate significant heterogeneity in soil composition and morphology across the study area, which is important for understanding heavy metal distribution, geochemical partitioning, and environmental behaviour within the different sequential extraction phases.

Table 1. Field Description and Geographic Coordinates of Soil Samples Collected from the Ikole–Itapaji Area, Southwestern Nigeria

S/N	Sample ID	Locality	Latitude	Longitude	Elevation (m)	Depth (m)	Description	Colour
1	SQ1	Igbona-Ile, Ikole 1	7°45'41.9"	05°28'49.8"	564	0.35	Laterite	Reddish brown
2	SQ2	Igbona-Ile, Ikole 2	7°45'33.8"	05°26'53.6"	558	0.30	Sandy clay	Brown
3	SQ3	Ikole 1	7°46'23.3"	05°27'48.0"	550	0.50	Reddish brown soil	Reddish brown
4	SQ4	Agbeyewa farm	7°45'14.9"	05°28'12.6"	52	0.36	Sandy clay	Brown
5	SQ5	Ikole 2	7°50'55.8"	05°26'52.6"	556	0.40	Lateritic sand	Brown

S/N	Sample ID	Locality	Latitude	Longitude	Elevation (m)	Depth (m)	Description	Colour
6	SQ6	Aba farm	7°50'04.8"	05°28'16.1"	588	0.60	Laterite	Reddish brown
7	SQ7	Ikole 3	7°59'57.6"	05°27'24.0"	533	0.50	Sand	Brown
8	SQ8	Aba Dam	7°55'36.1"	05°27'42.0"	491	0.25	Laterite	Reddish brown
9	SQ9	Esun	7°45'14.9"	05°28'12.6"	541	0.28	Sandy clay	Brown
10	SQ10	Agbeyewa Farm	7°56'21.0"	05°30'20.0"	453	0.50	Gravelly sand	Grayish brown
11	SQ11	Aba Farm, Itapaji	7°58'47.0"	05°33'34.4"	447	0.34	Gravelly sand	Brown
12	SQ12	Aba Farm	7°54'23.1"	05°28'00.9"	481	0.40	Clayey sand	Brown
13	SQ13	Omu	7°53'18.9"	05°27'42.3"	503	0.30	Sand	Brown
14	SQ14	Itapaji	7°52'49.9"	05°31'05.2"	501	0.35	Sandy loam	Dark brown
15	SQ15	Iyemero	7°45'52.6"	05°33'06.3"	586	0.30	Laterite	Reddish brown
16	SQ16	Odo- Oro	7°49'45.0"	05°31'39.9"	578	0.35	Gravelly clay	Brown
17	SQ17	Ikole 4	7°50'46.3"	05°33'20.5"	543	0.40	Gravelly sand	Brown

2.2 Regional Geological Setting

The study area is located within southwestern Nigeria, forming part of the Precambrian Basement Complex of the West African Craton. This crystalline basement terrain is distinct from the surrounding sedimentary basins, including the Sokoto Basin, Chad Basin, Bida Basin, and the Benue Trough, which are largely composed of Cretaceous to Tertiary sediments (Ojo et al., 2024). The southwestern region, including the Ikole–Itapaji axis, is dominated by crystalline rocks that have undergone extensive tectono-metamorphic evolution. The Nigerian Basement Complex evolved through multiple orogenic events, notably the Liberian, Eburnean, and Pan-African cycles, which resulted in widespread deformation, metamorphism, and granitoid emplacement (Adetunla et al., 2025). These processes led to the development of major lithological units, including the migmatite–gneiss complex, schist belts, and Pan-African granitoids. In the study area, migmatite–gneiss and granitic rocks are predominant, with minor metasedimentary occurrences.

Structurally, the area is characterized by well-developed faults, fractures, and foliations, predominantly trending NE–SW and NW–SE, reflecting the imprint of the Pan-African deformational event (Ogah & Abubakar, 2024). These structures are critical in controlling hydrothermal fluid flow and mineral deposition. Mineralization within the Basement Complex is commonly associated with quartz veins, pegmatites, and shear zones. The presence of granitic and pegmatitic intrusions within the Ikole–Itapaji area further suggests favourable conditions for mineralization. Recent studies have demonstrated the effectiveness of integrated geophysical methods in delineating such structurally controlled mineralized zones (Salako et al., 2024). The geological framework of the study area reflects a complex interplay of lithology and structure, providing a suitable environment for mineralization and justification for integrated geophysical and remote sensing investigations **(Fig. 1)**

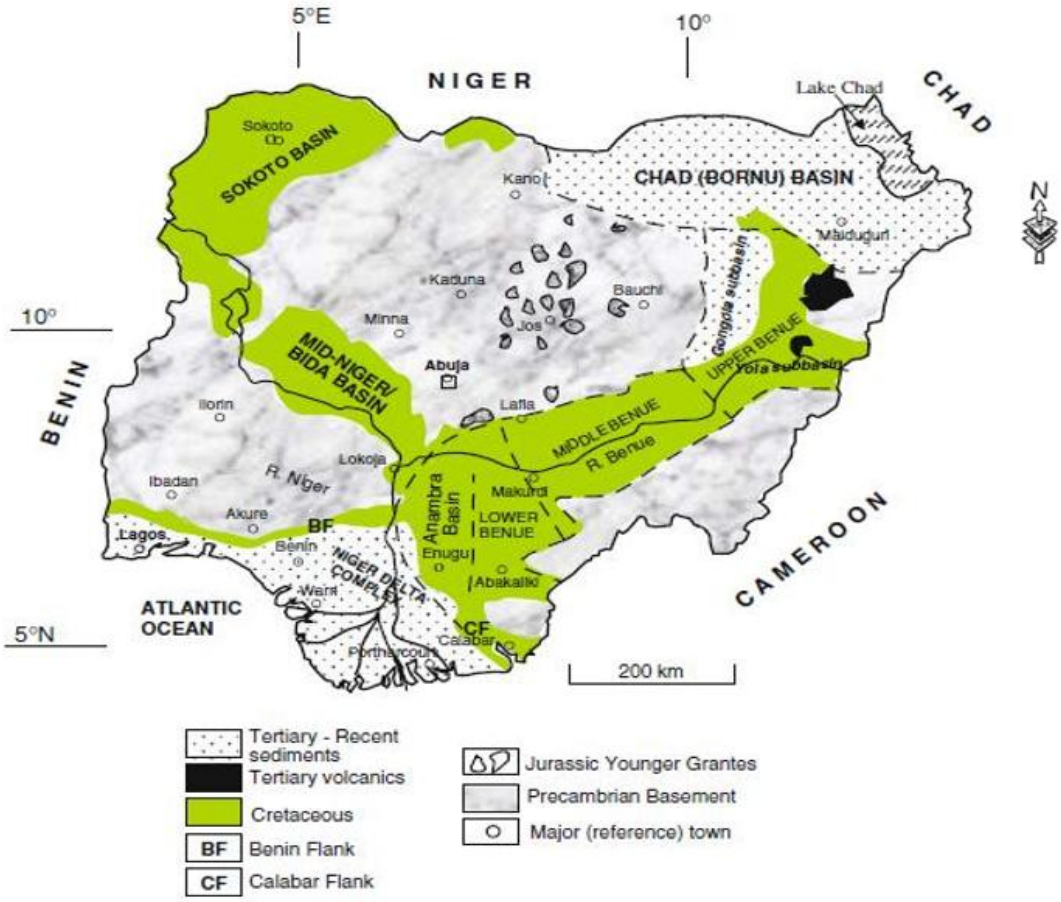

Figure 1: Geological map of Nigeria showing the distribution of major lithological units, including the Precambrian Basement Complex and surrounding sedimentary basins (Sokoto, Chad, Bida, and Benue Trough). The study area (Ikole–Itapaji, southwestern Nigeria) is located within the Basement Complex.

2.3 Geologic Map of the Study Area

The geological map of the study area reveals the major lithological units within the Precambrian Basement Complex of Southwestern Nigeria, particularly within the Ekiti basement terrain. The area has experienced complex tectonic, metamorphic, and magmatic activities associated mainly with the Pan-African orogeny (~600 ± 150 Ma) (Rahaman, 1988; Oyinloye, 2011). The dominant rock units include migmatite, granite gneiss, charnockite, and granodiorite.

Migmatite (Mg) occurs mainly in the southern and central portions around Ikole and Odo Oro. These rocks represent some of the oldest basement units and were formed through partial melting under high-grade metamorphic conditions. Granite gneiss (GG) is the most extensive lithology, occupying the northern, central, and western parts of the area, including Itapaji and Bolorunduro. These foliated granitic rocks are structurally competent and commonly host deformation features such as fractures and faults (Oyinloye, 2011).

Charnockite (Ch) occurs locally along the western margin of the study area and represents high-temperature granulite-facies rocks associated with deep crustal processes (Rahaman, 1988). Granodiorite (OGd) forms a major intrusive body

within the north-central part of the area and belongs to the Older Granite suite emplaced during the late stages of the Pan-African orogeny. These intrusions commonly occupy structurally weak within the basement complex (Oyinloye, 2011) (**Fig. 2**).

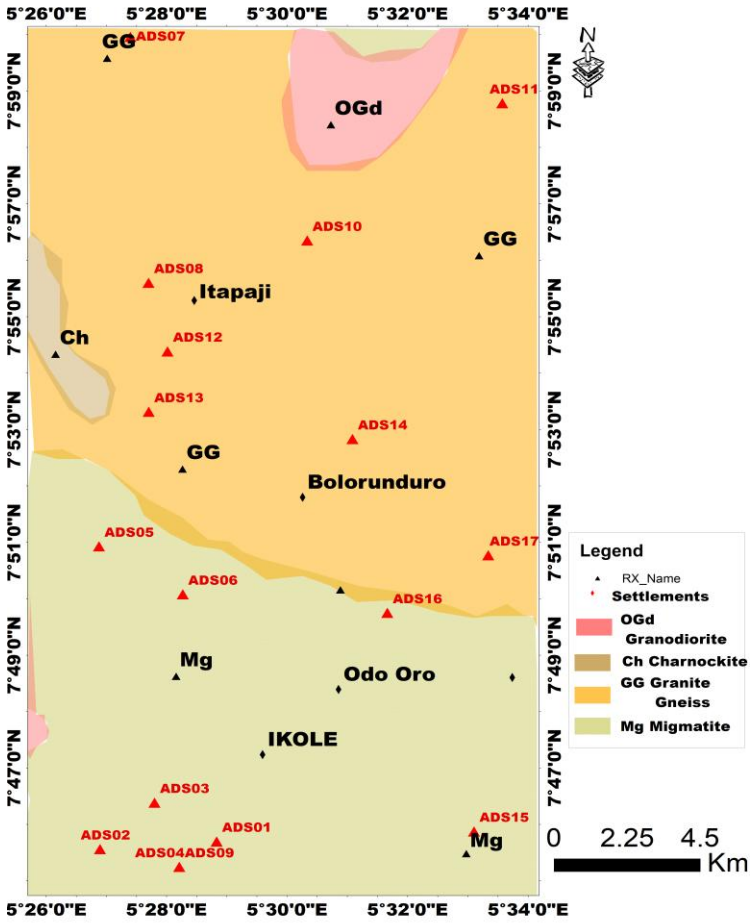

Figure 2: **Geological map of the study area after NGSA (2006). The map delineates the distribution of major lithological units and their spatial relationships. It provides a foundational framework for structural interpretation and mineral exploration within the study area.**

2.4 Sampling points from the study area

Figure 3 shows the spatial distribution of the seventeen soil sampling locations (SQ1–SQ17) within the Ikole–Itapaji area of Southwestern Nigeria, a section of the Precambrian Basement Complex characterized by prolonged tectonic, metamorphic, and magmatic evolution associated with the Pan-African orogeny (Rahaman, 1988; Oyinloye, 2011). The mapped area covers approximately 16 km (north–south) and 8 km (east–west), encompassing settlements such as Ikole, Itapaji, Odo-Oro, and Bolorunduro.

The sampling design follows a purposive distribution strategy to capture variability in lithology,

weathering intensity, drainage influence, and land-use activities, rather than relying on a strict grid system. A relatively higher concentration of sampling points occurs around the Ikole–Itapaji axis, reflecting its geological relevance, accessibility, and greater anthropogenic influence (Oyinloye, 2011).

Several sampling locations were deliberately positioned near drainage channels and low-lying terrains to evaluate the influence of surface runoff, leaching, and sediment transport on soil geochemistry. The underlying topography is moderately undulating, consisting of ridges, slopes, and valley systems typical of Basement Complex terrains. This geomorphological variation allows assessment of how relief controls weathering intensity and trace metal redistribution across different landscape positions.

In addition, the proximity of some sampling sites to cultivated lands and settlements provides insight into possible anthropogenic contributions to soil metal content, particularly through agricultural practices and land-use activities. Overall, the integration of topography, drainage features, and strategically distributed sampling points provides a strong framework for understanding the combined influence of geological, geomorphological, and human factors on heavy metal distribution in the Ikole–Itapaji area (Rahaman, 1988; Oyinloye, 2011).

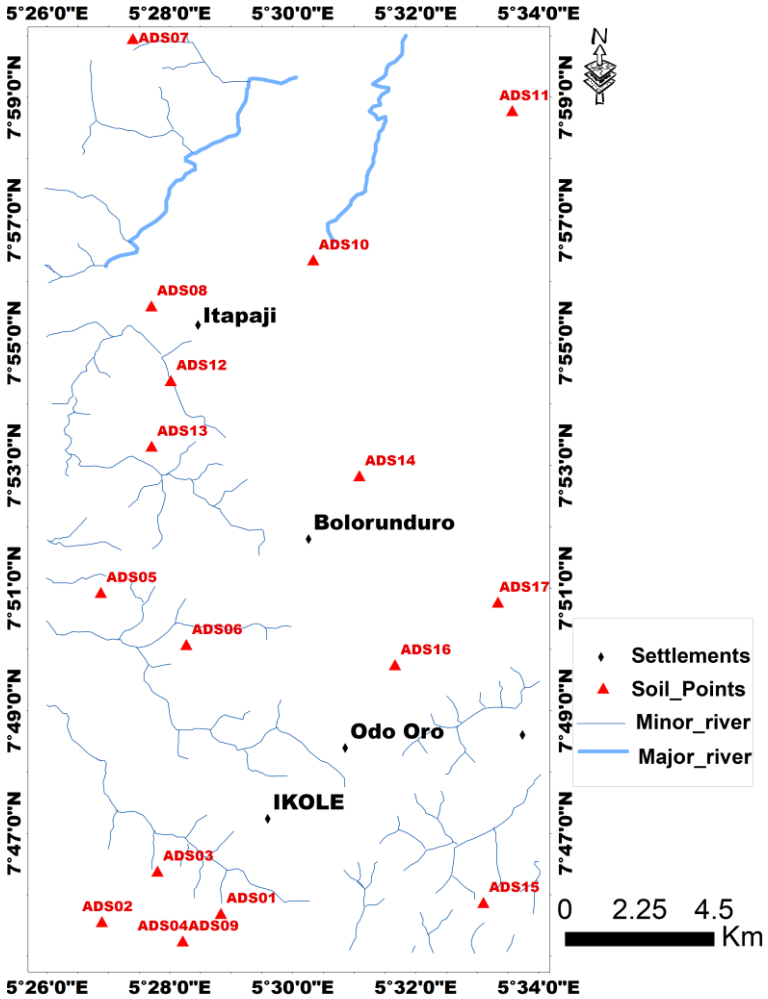

Figure 3. Drainage map of the study area showing the locations of sampled points used for geological, geochemical, and petrographic investigations.

3. 0 Materials and Methods

3.1 Sample Collection and Preparation

Soil/sediment samples were collected from selected locations within Ikole-Itapaji. The samples were obtained at shallow depths to represent the surficial geochemical environment of the study area. Each sample was air-dried at room temperature, gently disaggregated, and sieved to obtain the <63 µm fraction, which is known to retain higher concentrations of trace metals due to its large surface area and adsorption capacity.

A representative mass of 1.0 g of each prepared sample was weighed into clean centrifuge tubes for sequential extraction analysis.

3.2 Sequential Extraction Procedure

A seven-step sequential extraction procedure, modified from the widely adopted Tessier extraction scheme, was employed to partition metals into operationally defined geochemical fractions. This approach enables the differentiation of metals based on their binding strength and geochemical associations within sediments and soils. The procedure was designed to extract metals associated with water-soluble, exchangeable, carbonate-bound, Fe–Mn oxide-bound, organic-bound, sulfide/strongly bound, and residual phases.

Sequential extraction techniques have been widely applied in recent studies to evaluate the mobility, bioavailability, and environmental risk of trace metals in soils and sediments, as they provide more reliable information than total metal concentrations alone (De Matteis et al., 2023; Bouazizi et al., 2023). The method operates on the principle of selective dissolution, where specific reagents target distinct mineralogical or geochemical phases, allowing for detailed characterization of metal partitioning (Doi et al., 2023). Recent modifications of the classical Tessier procedure have demonstrated improved efficiency, reproducibility, and applicability across diverse environmental matrices, including contaminated sediments and mining-impacted soils (Çelebi, 2024; Souza et al., 2024).

The adopted seven-step scheme provides enhanced resolution of metal speciation, particularly in distinguishing weakly bound fractions from those strongly incorporated within mineral lattices, thereby offering critical insights into both environmental behavior and mineralization processes.

The extraction steps were carried out as follows:

Phase 1: Water-Soluble Fraction
Twenty milliliters (20 mL) of deionized water was added to 1.0 g of sample and agitated for 1 hour at room temperature. The mixture was centrifuged, and the supernatant was decanted for analysis.

Phase 2: Exchangeable Fraction
Twenty milliliters (20 mL) of 1 M $MgCl_2$ solution was added to the residue from Phase 1 and shaken for 1 hour. The mixture was centrifuged, and the extract was collected.

Phase 3: Carbonate-Bound Fraction
Twenty milliliters (20 mL) of 1 M sodium acetate (NaOAc) adjusted to pH 5 was added to the residue from Phase 2 and shaken for 5 hours. After centrifugation, the extract was filtered and preserved.

Phase 4: Fe–Mn Oxide (Reducible) Fraction
Twenty milliliters (20 mL) of hydroxylamine hydrochloride ($NH_2OH{\cdot}HCl$) solution was added to the residue from Phase 3 and heated at approximately 95°C for 2 hours with intermittent agitation. The mixture was cooled, centrifuged, and the extract was collected.

Phase 5: Organic Matter-Bound Fraction
Ten milliliters (10 mL) of acidified hydrogen peroxide (H_2O_2) was added to the residue from Phase 4 and heated at 85°C for 2 hours. A second aliquot of 10 mL H_2O_2 was added, followed by repeated heating. After cooling, 20 mL of ammonium acetate (NH_4OAc) was added, and the mixture was shaken

for 30 minutes before centrifugation and collection of the extract.

Phase 6: Sulfide/Strongly Bound Fraction
Fifteen milliliters (15 mL) of concentrated nitric acid (HNO_3) was added to the residue from Phase 5 and heated gently to near dryness. The residue was cooled, diluted, centrifuged, and the extract was collected.

Phase 7: Residual Fraction
The final residue was digested using a mixture of hydrofluoric acid (HF), perchloric acid ($HClO_4$), and nitric acid (HNO_3) until complete dissolution was achieved. The digest was appropriately diluted for analysis.

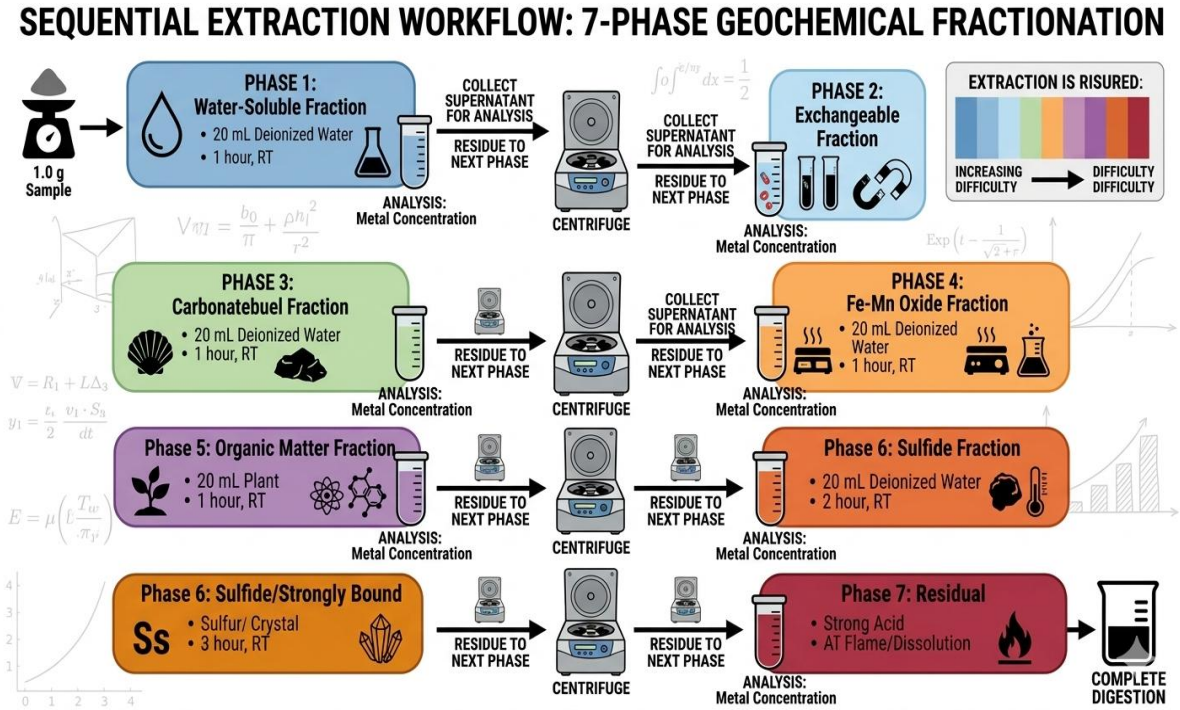

3.3 Geochemical Pollution Indices

Trace metal concentrations were determined using **Atomic Absorption Spectrophotometry (AAS)** (Buck Scientific Model 205A) with an air–acetylene flame. Calibration standards were prepared using appropriate matrix-matched solutions to ensure analytical accuracy.

For each fraction, the supernatant was diluted where necessary (typically 20–50×), and concentrations were obtained from calibration curves. All analyses were conducted in triplicate, and reagent blanks were included to ensure quality control.

For total metal determination (residual fraction), samples were subjected to strong acid digestion using HF–$HClO_4$–HNO_3 mixtures to ensure complete dissolution of silicate matrices, following standard geochemical digestion protocols.

3.3.1 Ecological Risk Index (ERI)

- The Ecological Risk Index (ERI) was used to evaluate the potential ecological risk posed

by heavy metals in the study area. It was calculated in two steps:

- Er = Tr × CF
- $ERI = \Sigma Er$ (1)
- where:
  Er represents the potential ecological risk factor for each metal,
  Tr represents the toxic response factor of each metal,
  CF represents the contamination factor.
- Common toxic response factors include Cd = 30, Pb = 5, Cu = 5, Ni = 5, Co = 5, Cr = 2, and Zn = 1.
- Higher ERI values indicate greater ecological risk and potential harm to aquatic and terrestrial ecosystems.

3.3.2 Mobility Factor (MF)

The **Mobility Factor (MF)** was used to evaluate the potential mobility and bioavailability of metals in the studied samples. It was calculated using the relationship:

$$MF\ (\%) = [(F1 + F2 + F3) / (F1 + F2 + F3 + F4 + F5 + F6 + F7)] \times 100 \quad (2)$$

where:

- F1–F3 represent the more mobile fractions (water-soluble, exchangeable, carbonate-bound),
- F4–F7 represent the more stable fractions.

Higher MF values indicate greater environmental mobility and potential ecological risk

Table 2. Average shale values of selected heavy metals used as geochemical background concentrations for pollution assessment in the study area (Turekian and Wedepohl, 1961).

S/N	Metal	Shale Value (mg/kg)
1	Fe	47,200
2	Mn	850
3	Pb	20
4	Cu	45
5	Zn	95
6	Ni	68
7	Co	19
8	Cr	90
9	Cd	0.3

4.0 Results and discussion

4.1 Water-soluble phase

The water-soluble phase represents the most mobile and bioavailable fraction of metals in soils and sediments, and it is typically very low in natural systems due to strong mineral binding (Kabata-Pendias, 2011; Alloway, 2013).

Results in **Table 3a** show generally low concentrations of all metals across samples (SQ1–SQ17), indicating limited dissolution into pore

water. Fe records the highest values (2.873–7.427 mg/kg), reflecting relatively higher geochemical reactivity but still low mobility due to strong association with silicate and oxide minerals. Mn ranges from 1.742–3.128 mg/kg, showing slight variation linked to redox sensitivity (Reimann & de Caritat, 2012). Cu (0.163–0.742 mg/kg) and Zn (0.126–0.627 mg/kg) are low, suggesting natural weathering control, while Pb (0.049–0.098 mg/kg) and Cd (0.002–0.007 mg/kg) indicate minimal contamination and strong retention in solid phases. Ni, Co, and Cr also remain consistently low across samples.

The statistical summary in **Table 3b** confirms low variability, with mean concentrations ordered as Fe > Mn > Cu ≈ Zn > Pb > Co ≈ Ni > Cr > Cd. This indicates dominance of lithogenic control with very limited metal mobility. The spatial distribution shown in **Figure 4** (cluster column chart**)** supports these observations, clearly illustrating the dominance of Fe and Mn across all samples. At the same time, other metals remain uniformly low with no distinct spatial anomaly. The clustering pattern confirms that variations are minor and do not reflect pollution hotspots but natural geochemical background levels.

Overall, the combined interpretation of **Table 3a, Table 3b, and Figure 4** indicates low mobility, weak aqueous dispersion, and strong lithogenic control of metals in the water-soluble phase, with negligible environmental risk under current conditions.

Table 3a. Heavy metals concentration in the water-soluble phase (mg/kg) of sediments/soils from the Ikole–Itapaji area, Southwestern Nigeria. This fraction represents the most mobile and immediately bioavailable portion of trace metals, reflecting their potential short-term environmental availability and mobility in the near-surface environment.

Samples	Fe (mg/Kg)	Mn (mg/Kg)	Pb (mg/Kg)	Cu (mg/Kg)	Zn (mg/Kg)	Ni (mg/Kg)	Co (mg/Kg)	Cr (mg/Kg)	Cd (mg/Kg)
SQ 1	6.321	2.087	0.077	0.681	0.572	0.054	0.062	0.023	0.004
SQ 2	6.128	2.063	0.072	0.631	0.509	0.059	0.063	0.021	0.003
SQ 3	7.427	3.108	0.083	0.724	0.592	0.063	0.069	0.028	0.005
SQ 4	7.129	3.099	0.081	0.711	0.579	0.061	0.066	0.025	0.005
SQ 6	5.873	2.145	0.094	0.742	0.582	0.063	0.067	0.029	0.006
SQ7	4.568	1.958	0.064	0.465	0.368	0.043	0.048	0.016	0.003
SQ 8	6.409	2.056	0.076	0.641	0.539	0.052	0.063	0.022	0.004
SQ 10	2.873	1.742	0.049	0.163	0.126	0.034	0.037	0.013	0.002
SQ 11	3.208	1.839	0.056	0.218	0.189	0.041	0.045	0.015	0.003
SQ 12	5.175	2.094	0.086	0.598	0.565	0.061	0.057	0.024	0.005
SQ 13	5.387	2.109	0.087	0.605	0.591	0.063	0.054	0.026	0.005
SQ 14	6.125	2.135	0.092	0.676	0.608	0.067	0.061	0.029	0.006
SQ 15	7.105	3.128	0.091	0.624	0.573	0.056	0.054	0.031	0.006
SQ 16	5.891	2.207	0.095	0.673	0.606	0.065	0.059	0.034	0.007
SQ 17	5.006	1.876	0.098	0.659	0.627	0.064	0.062	0.033	0.007

Table 3b. Statistical summary of the heavy metals concentration in the water-soluble phase (mg/kg). This table presents the minimum, maximum, and mean concentrations of the selected metals across all samples in the study area. It provides a simplified statistical overview of metal distribution and mobility within the most labile geochemical fraction of the soil–sediment system.

Metal	Fe	Mn	Pb	Cu	Zn	Ni	Co	Cr	Cd
Min	2.873	1.742	0.049	0.163	0.126	0.034	0.037	0.013	0.002
Max	7.427	3.128	0.098	0.742	0.627	0.067	0.069	0.034	0.007
Mean	5.642	2.243	0.080	0.587	0.508	0.056	0.058	0.025	0.005

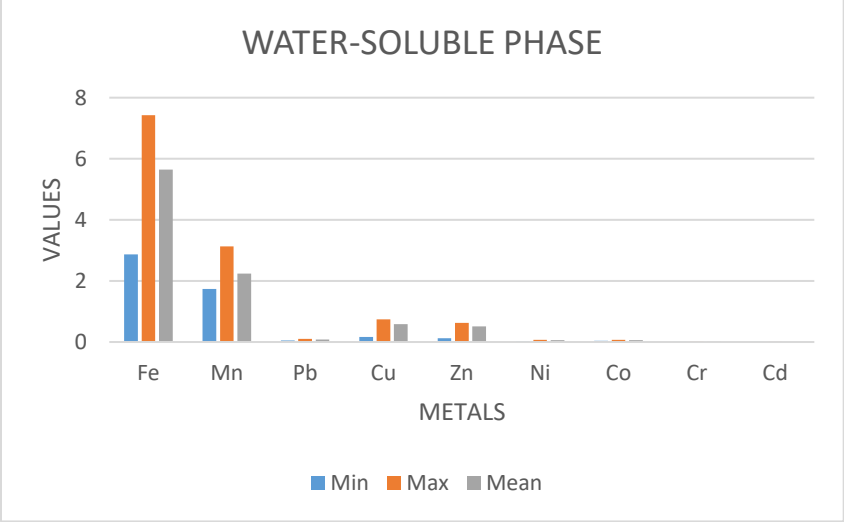

Figure 4. Cluster column chart of heavy metal concentrations in the water-soluble phase (mg/kg). The figure illustrates the comparative distribution of selected metals across all samples, highlighting variations in their mobility and relative abundance within the most labile geochemical fraction.

4.2 The exchangeable phase

The exchangeable phase consists of metals weakly adsorbed to soil surfaces and is environmentally important because such metals can be released under changes in pH, ionic strength, or competing ions (Kabata-Pendias, 2011; Alloway, 2013).

Table 4a shows higher metal concentrations than the water-soluble phase, indicating stronger but reversible adsorption to soil exchange sites. Fe is dominant (5.731–10.742 mg/kg), reflecting strong association with clay and oxide minerals. Mn (1.342–3.127 mg/kg) shows moderate variability linked to redox sensitivity (Alloway, 2013).

Cu (0.279–0.967 mg/kg) and Zn (0.261–0.886 mg/kg) are moderately retained, while Pb (0.082–0.146 mg/kg) and Cd (0.004–0.029 mg/kg) remain low but slightly enriched, indicating potential mobility under acidic conditions. Ni, Co, and Cr are consistently low, reflecting partial release from primary minerals. **Table 4b** shows the mean order:
Fe > Mn > Cu > Zn > Pb > Ni > Co > Cr > Cd, confirming Fe and Mn dominance.

Spatially, SQ3, SQ4, SQ14, SQ15, and SQ17 show higher values, while SQ10 is the lowest, suggesting natural lithological control rather than contamination. This pattern is supported by **Figure 5**, which

highlights clear Fe–Mn dominance, moderate Cu–Zn clustering, and uniformly low Pb, Cd, Ni, Co, and Cr across samples.

Overall, the exchangeable phase exhibits moderate metal retention and limited mobility, controlled primarily by clay minerals and organic matter. The presence of Pb and Cd, though low, indicates potential sensitivity to environmental changes such as acidification (Kabata-Pendias, 2011; Alloway, 2013).

Table 4a: Exchangeable phase of the heavy metal concentrations in soil samples (mg/kg). The table presents the distribution of Fe, Mn, Pb, Cu, Zn, Ni, Co, Cr, and Cd across all sampling locations, reflecting metals weakly bound to soil exchange sites and their potential environmental mobility.

Samples	Fe (mg/Kg)	Mn (mg/Kg)	Pb (mg/Kg)	Cu (mg/Kg)	Zn **(mg/Kg)**	Ni (mg/Kg)	Co (mg/Kg)	Cr (mg/Kg)	Cd (mg/Kg)
SQ 1	8.084	1.875	0.098	0.789	0.701	0.072	0.071	0.031	0.007
SQ 2	8.005	1.802	0.097	0.712	0.685	0.073	0.069	0.032	0.005
SQ 3	10.742	2.085	0.102	0.826	0.732	0.081	0.075	0.037	0.029
SQ 4	10.488	2.016	0.108	0.813	0.735	0.085	0.076	0.037	0.028
SQ 6	6.402	2.073	0.112	0.839	0.784	0.082	0.073	0.042	0.009
SQ7	6.023	1.762	0.082	0.619	0.586	0.065	0.059	0.025	0.005
SQ 8	8.787	1.904	0.126	0.804	0.721	0.075	0.073	0.034	0.026
SQ 10	5.731	1.342	0.085	0.279	0.261	0.067	0.072	0.026	0.004
SQ 11	6.174	1.563	0.096	0.351	0.31	0.071	0.072	0.029	0.005
SQ 12	7.787	2.012	0.113	0.801	0.721	0.094	0.087	0.038	0.009
SQ 13	7.819	2.105	0.109	0.799	0.726	0.097	0.085	0.042	0.01
SQ 14	8.534	3.083	0.138	0.902	0.846	0.102	0.095	0.051	0.017
SQ 15	10.231	3.127	0.146	0.927	0.872	0.117	0.102	0.054	0.021
SQ 16	7.118	2.105	0.128	0.942	0.839	0.112	0.11	0.059	0.028
SQ 17	6.104	2.098	0.131	0.967	0.886	0.132	0.121	0.061	0.026

Table 4b: Statistical summary of the heavy metals concentration in the exchangeable phase (mg/kg). This table presents the minimum, maximum, and mean concentrations of selected metals across all samples in the exchangeable fraction. It highlights the variability and relative mobility of metals weakly bound to soil exchange sites, which are potentially available for environmental release.

Metal	**Fe**	**Mn**	**Pb**	**Cu**	**Zn**	**Ni**	**Co**	**Cr**	**Cd**
Min	5.731	1.342	0.082	0.279	0.261	0.065	0.059	0.025	0.004
Max	10.742	3.127	0.146	0.967	0.886	0.132	0.121	0.061	0.029
Mean	7.869	2.064	0.111	0.758	0.694	0.088	0.083	0.040	0.015

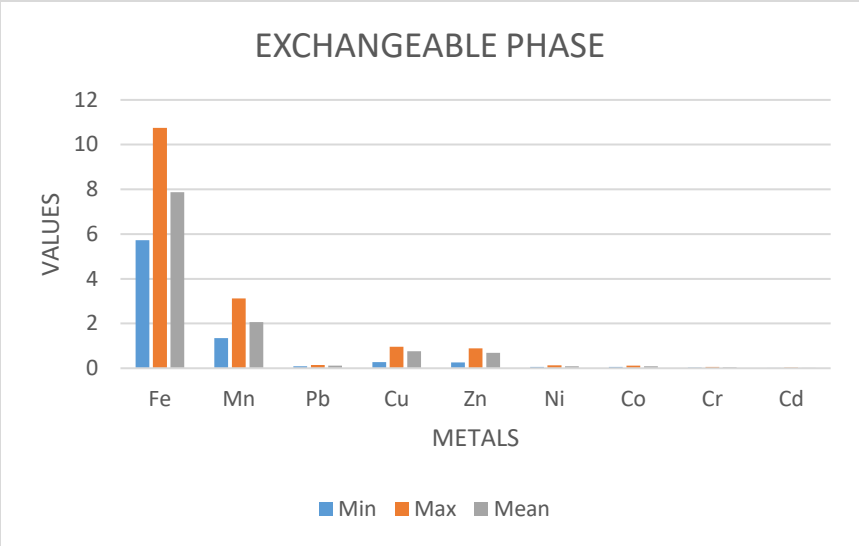

Figure 5. Cluster column chart of heavy metal concentrations in the exchangeable phase (mg/kg). The figure illustrates the comparative distribution of metals across all samples in the exchangeable fraction, highlighting variations in their relative mobility and binding strength to soil exchange sites.

4.3 The carbonate-bound phase

The carbonate-bound phase comprises metals associated with carbonate minerals and is sensitive to pH changes, particularly under acidic conditions where dissolution can release bound metals (Kabata-Pendias, 2011; Alloway, 2013).

Table 5a shows a clear increase in metal concentrations compared to earlier fractions, indicating stronger incorporation into carbonate phases. Fe (36.325–66.488 mg/kg) and Mn (23.728–38.019 mg/kg) dominate, reflecting their affinity for co-precipitation with carbonates. Zn (12.101–19.807 mg/kg) and Cu (1.112–3.213 mg/kg) show moderate enrichment, while Pb (1.025–3.832 mg/kg) indicates stable carbonate association. Ni, Co, and Cr occur at lower but consistent levels, and Cd remains low (0.054–0.121 mg/kg). The statistical summary in **Table 5b** confirms the trend: Fe > Mn > Zn > Pb > Cu > Ni > Co > Cr > Cd

Spatially, higher values in SQ3, SQ4, and SQ15 contrast with lower concentrations in SQ10, reflecting lithological variability rather than contamination. This pattern is supported by **Figure 6**, which highlights Fe–Mn dominance, moderate Zn–Cu enrichment, and consistently lower levels of other metals across samples (Müller (1969). Overall, the carbonate-bound phase represents a moderately stable metal reservoir with potential mobility under acidic conditions, although current distributions indicate strong lithogenic control.

Table 5a. Heavy metal concentrations in the carbonate-bound phase (mg/kg). The table shows the distribution of metals associated with carbonate minerals across all samples, reflecting their relative stability and potential release under acidic environmental conditions.

Samples	Fe (mg/Kg)	Mn (mg/Kg)	Pb (mg/Kg)	Cu (mg/Kg)	Zn (mg/Kg)	Ni (mg/Kg)	Co (mg/Kg)	Cr (mg/Kg)	Cd (mg/Kg)
SQ 1	40.129	25.207	2.279	2.439	13.226	2.147	1.701	0.531	0.069
SQ 2	41.052	25.422	2.142	2.197	13.055	2.132	1.626	0.625	0.065
SQ 3	65.246	37.529	3.217	2.826	18.614	2.704	2.002	0.954	0.089
SQ 4	66.488	38.019	3.832	3.213	18.901	3.125	2.106	1.005	0.103
SQ 6	38.615	24.234	1.715	2.327	13.178	2.362	1.448	0.603	0.059
SQ7	38.247	24.127	1.665	2.401	13.218	2.295	1.353	0.616	0.055
SQ 8	41.271	25.431	3.102	2.424	13.286	2.149	1.747	1.103	0.072
SQ 10	36.325	23.728	1.025	1.112	12.521	1.891	0.829	0.518	0.054
SQ 11	37.623	24.061	2.611	2.103	12.101	2.047	1.521	0.556	0.055
SQ 12	39.114	25.716	3.112	2.518	12.224	2.104	1.687	0.738	0.069
SQ 13	38.864	24.612	3.109	2.429	12.138	2.049	1.716	0.742	0.071
SQ 14	41.451	26.128	2.234	2.657	13.441	2.162	1.392	0.671	0.077
SQ 15	46.539	37.423	3.627	2.985	19.807	3.127	2.108	1.054	0.121
SQ 16	41.318	25.035	2.512	2.548	13.033	2.102	1.711	1.005	0.098
SQ 17	38.712	24.291	2.271	2.462	12.987	1.937	1.491	0.657	0.097

Table 5b. Statistical summary of the heavy metals in the carbonate-bound phase (mg/kg). The table presents the minimum, maximum, and mean concentrations of metals associated with carbonate fractions, highlighting their relative enrichment and stability within this geochemical phase.

Metal	Fe	Mn	Pb	Cu	Zn	Ni	Co	Cr	Cd
Min	36.325	23.728	1.025	1.112	12.101	1.891	0.829	0.518	0.054
Max	66.488	38.019	3.832	3.213	19.807	3.127	2.108	1.103	0.121
Mean	43.580	26.998	2.630	2.450	13.915	2.235	1.629	0.758	0.078

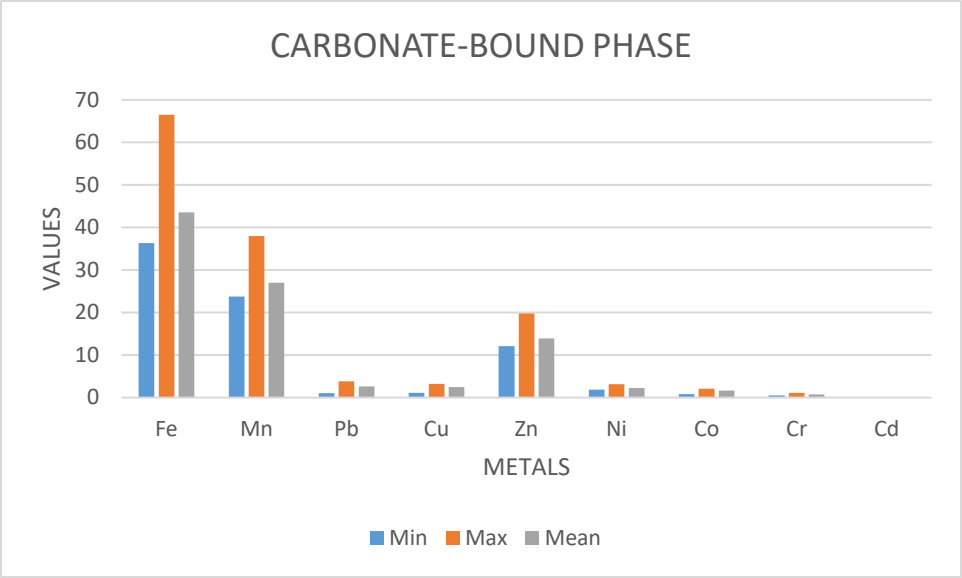

Figure 6. Cluster column chart of the heavy metal concentrations in the carbonate-bound phase (mg/kg). The figure illustrates the comparative distribution of metals across all samples, highlighting their relative enrichment and association with carbonate minerals within this geochemical fraction.

4.4 The Fe–Mn oxide phase

Table 6a and 6b present the distribution and statistical summary of heavy metals associated with the Fe–Mn oxide fraction across the studied soil samples. This geochemical phase is particularly important because iron and manganese oxides are known to have strong adsorption capacities and therefore act as major sinks for trace metals in soil environments (Kabata-Pendias, 2011; Alloway, 2013). The results show that Fe and Mn occur in relatively high concentrations across all samples, with Fe ranging from 303.187 to 476.031 mg/kg and Mn from 139.204 to 267.163 mg/kg. These elevated values reflect the dominance of Fe–Mn oxides in controlling metal retention and indicate strong scavenging of trace elements during secondary soil-forming processes (Hakanson (1980).

Among the trace metals, Zn shows comparatively higher concentrations (54.584–77.129 mg/kg), followed by Pb (16.623–36.125 mg/kg), Cu (11.197–22.957 mg/kg), and Ni (16.352–26.103 mg/kg). Co, Cr, and Cd occur at lower but still significant levels, indicating variable affinity for Fe–Mn oxide surfaces. The highest metal loadings are observed in samples SQ3, SQ4, and SQ15, suggesting localized enrichment possibly linked to lithological variation or enhanced adsorption under specific geochemical conditions Wei & Yang, (2010). In contrast, samples such as SQ10 consistently record the lowest concentrations, indicating weaker metal retention capacity in those locations (Birth (2003).

The statistical summary (Table 4b) further confirms the strong geochemical association of metals with Fe–Mn oxides, with mean concentrations following the order Fe > Mn > Zn > Pb > Cu > Ni > Co > Cr > Cd. The relatively high mean values of Zn, Pb, and Cu suggest significant anthropogenic influence superimposed on natural geochemical processes. Overall, the Fe–Mn oxide fraction plays a critical role in controlling metal mobility and redistribution in the study area, as these oxides can effectively adsorb and immobilize trace metals under varying redox conditions (Tessier et al., 1979; Wei & Yang, 2010).

Table 6a: Heavy metal concentrations in the Fe–Mn oxide phase (mg/kg). The table presents the distribution of metals associated with iron and manganese oxides across all samples, reflecting their strong adsorption capacity and role as key geochemical sinks for trace elements.

Samples	Fe	Mn	Pb	Cu	Zn	Ni	Co	Cr	Cd
	(mg/Kg)	(mg/Kg)	(mg/Kg)	(mg/Kg)	**(mg/Kg)**	(mg/Kg)	(mg/Kg)	(mg/Kg)	(mg/Kg)
SQ 1	354.813	152.227	25.711	13.403	63.866	19.181	10.271	6.361	0.621
SQ 2	361.558	175.129	22.019	15.019	63.545	20.196	11.287	6.185	0.657
SQ 3	435.209	237.214	33.277	20.236	74.091	22.573	14.263	9.159	1.872
SQ 4	446.513	241.116	35.332	21.873	77.129	26.103	14.742	10.015	1.983
SQ 6	362.145	154.434	26.072	12.615	63.071	20.032	10.481	5.235	0.598
SQ7	358.903	149.828	21.612	13.211	63.242	18.269	9.593	6.062	0.615
SQ 8	371.874	185.401	26.128	14.029	70.008	20.542	11.792	8.187	1.328
SQ 10	303.187	139.204	16.623	11.197	54.584	16.352	6.282	4.815	0.574
SQ 11	337.217	144.436	18.217	12.018	58.611	19.142	8.027	5.251	0.591
SQ 12	349.812	147.164	23.712	16.182	62.202	20.017	10.019	6.131	0.691
SQ 13	345.875	147.119	23.389	16.429	62.138	20.049	9.948	5.782	0.711
SQ 14	360.158	176.524	25.304	15.173	63.493	21.366	11.097	7.176	0.877
SQ 15	476.031	267.163	36.125	22.957	75.937	25.183	13.162	10.254	2.021
SQ 16	361.521	155.003	22.574	14.348	64.113	19.179	11.201	7.012	0.798
SQ 17	338.019	142.401	17.753	12.967	59.285	18.331	10.096	8.954	0.917

Table 6b: Statistical summary of the heavy metals concentration in the Fe–Mn oxide phase (mg/kg). The table shows the minimum, maximum, and mean concentrations of metals bound to Fe–Mn oxides, highlighting their significant enrichment and strong affinity for adsorption within this geochemical fraction.

Metal	**Fe**	**Mn**	**Pb**	**Cu**	**Zn**	**Ni**	**Co**	**Cr**	**Cd**
Min	303.187	139.204	16.623	11.197	54.584	16.352	6.282	4.815	0.574
Max	476.031	267.163	36.125	22.957	77.129	26.103	14.742	10.254	2.021
Mean	370.456	173.958	24.790	15.977	65.554	20.454	10.751	7.122	0.923

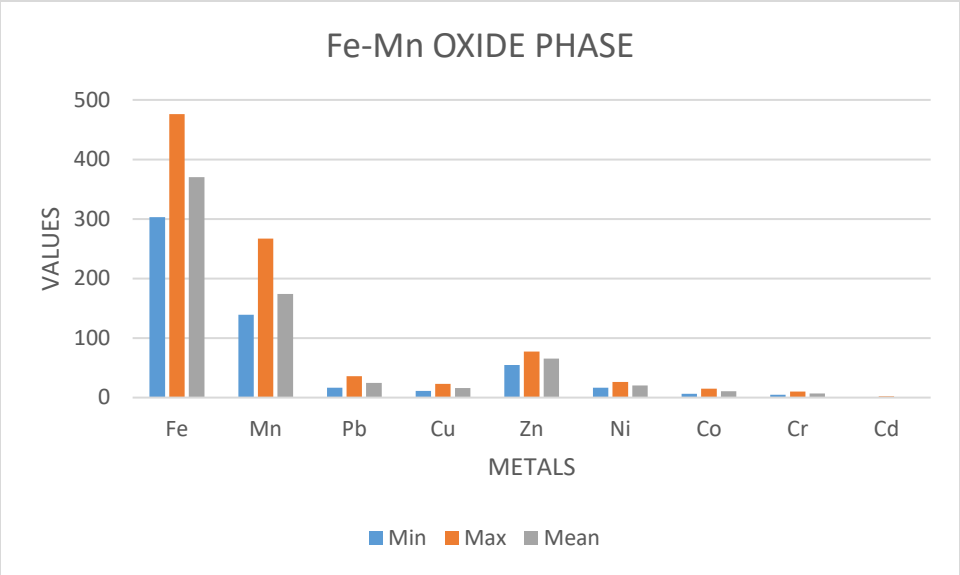

Figure 7. Cluster column chart of the heavy metal concentrations in the Fe–Mn oxide phase (mg/kg). The figure illustrates the comparative distribution of metals across all samples, highlighting strong enrichment and adsorption of trace elements onto Fe–Mn oxide phases within the study area.

4.5 The organic matter–bound phase

The organic matter–bound phase represents metals complexed with humic substances, decomposed organic residues, and microbial materials, and it acts as an important intermediate sink controlling metal retention and delayed release during organic matter decomposition. In tropical soils, this fraction is enhanced by high organic turnover and redox fluctuations, which promote metal–organic complex formation (Kaiser &Kalbitz, 2012; Liu et al., 2022).

From **Table 7a**, Fe shows the highest concentrations (148.854–356.163 mg/kg), indicating strong complexation with organic ligands. Mn (55.772–89.112 mg/kg) also shows appreciable association, reflecting its redox-sensitive behavior influenced by organic matter (Liu et al., 2022). Among trace metals, Cu (14.158–24.486 mg/kg) and Zn (24.128–40.372 mg/kg) are relatively enriched, confirming their strong affinity for organic functional groups. Pb (9.926–16.562 mg/kg) and Cd (0.414–1.221 mg/kg) occur at lower levels but remain environmentally important due to their potential remobilization during organic matter decomposition.

Ni, Co, and Cr show moderate association with organic matter, suggesting partial complexation and mixed control by both organic and mineral phases. The statistical summary in **Table 7b** confirms the dominance order: Fe > Mn > Zn > Cu > Ni ≈ Pb > Co > Cr > Cd, highlighting Fe and Mn as the major contributors to this fraction (Hakanson (1980).

Spatially, higher concentrations in SQ3, SQ4, and SQ15 suggest zones with stronger organic matter influence, while lower values in SQ6 and SQ10 reflect weaker organic binding Birth (2003). **Figure 8** shows a similar pattern, with Fe and Mn dominating, followed by Cu and Zn, while Pb, Cd, Ni, Co, and Cr remain comparatively low.

Overall, this phase indicates that organic matter plays a key role in stabilizing metals—especially Cu, Zn, Fe, and Mn—while also serving as a potential secondary source under decomposition or changing redox conditions (Alloway, 2013; Kaiser & Kalbitz, 2012).

Table 7a: Heavy metals concentrations in the organic matter–bound phase (mg/kg). The table shows the distribution of metals associated with organic matter across all samples, reflecting their affinity for organic complexation and potential release during organic matter decomposition.

Samples	Fe (mg/Kg)	Mn (mg/Kg)	Pb (mg/Kg)	Cu (mg/Kg)	Zn (mg/Kg)	Ni (mg/Kg)	Co (mg/Kg)	Cr (mg/Kg)	Cd (mg/Kg)
SQ 1	182.012	75.224	12.172	20.032	33.213	12.817	6.915	5.503	0.453
SQ 2	181.654	78.127	13.181	20.215	33.158	13.102	6.429	6.232	0.485
SQ 3	335.147	87.225	14.137	22.864	37.685	16.214	8.105	6.954	0.981
SQ 4	341.401	89.112	16.562	23.509	40.021	18.121	9.012	7.051	1.128
SQ 6	164.319	64.435	10.345	15.861	27.183	10.129	4.971	4.672	0.429
SQ7	168.247	64.247	10.631	15.539	28.011	10.216	5.056	4.956	0.433
SQ 8	189.074	81.236	13.123	20.421	33.786	13.014	6.747	6.143	0.472
SQ 10	148.854	55.772	9.926	14.158	24.128	8.997	4.635	4.329	0.414
SQ 11	152.627	57.201	10.011	15.141	25.091	9.089	4.921	4.457	0.425
SQ 12	169.612	65.236	11.162	16.214	25.274	10.176	5.068	4.781	0.446
SQ 13	169.881	64.837	11.134	16.452	25.181	10.089	5.112	8.714	0.451
SQ 14	180.575	76.294	12.634	21.052	32.846	12.763	6.557	5.773	0.472
SQ 15	356.163	87.826	15.663	24.486	40.372	18.522	9.138	7.074	1.221
SQ 16	185.052	75.135	12.246	20.415	33.325	13.012	6.751	6.028	0.482
SQ 17	168.176	65.095	10.773	15.404	28.197	10.332	6.904	6.193	0.462

Table 7b: Statistical summary of the heavy metals in the organic matter–bound phase (mg/kg). The table presents the minimum, maximum, and mean concentrations of metals associated with organic matter, indicating their degree of complexation and relative stability within this geochemical fraction.

Metal	Fe	Mn	Pb	Cu	Zn	Ni	Co	Cr	Cd
Min	148.854	55.772	9.926	14.158	24.128	8.997	4.635	4.329	0.414
Max	356.163	89.112	16.562	24.486	40.372	18.522	9.138	8.714	1.221
Mean	206.186	72.467	12.247	18.784	31.165	12.440	6.421	5.924	0.584

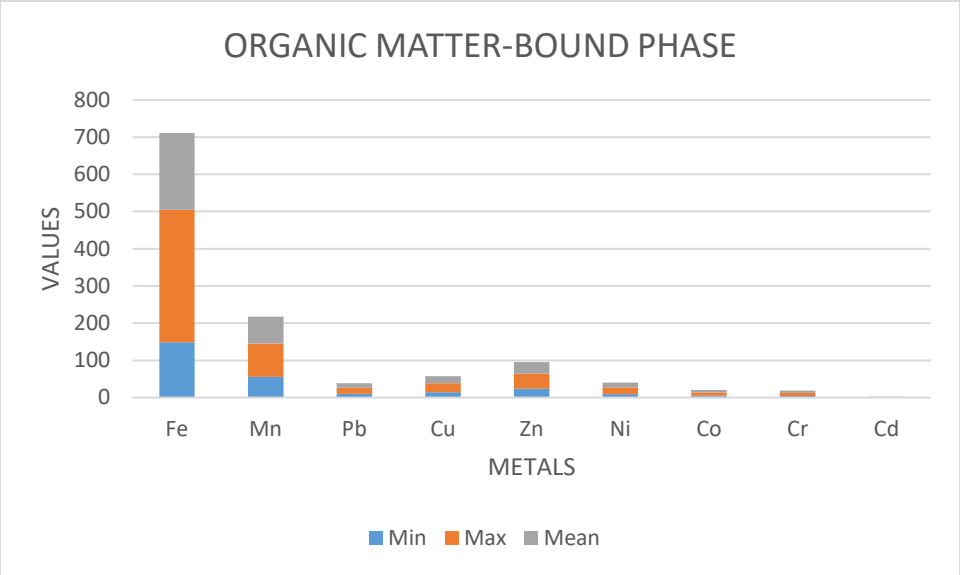

Figure 8. Cluster column chart of the heavy metal concentrations in the organic matter–bound phase (mg/kg). The figure illustrates the distribution of metals across all samples, highlighting their association with organic matter and relative enrichment through complexation with organic ligands.

4.6 The sulfide/strongly bound phase

The sulfide/strongly bound phase represents metals incorporated into sulfide minerals and resistant mineral lattices, and it is generally regarded as the most stable and least mobile fraction in sequential extraction studies. Metals in this fraction are only released under strong oxidizing conditions, making it a long-term geochemical sink for trace elements in soils and sediments (Tessier et al., 1979;).

From **Table 8a**, Fe shows the highest concentrations (184.382–353.506 mg/kg), indicating strong incorporation into resistant and sulfide-related mineral phases (Birth (2003). Mn (75.148–150.084 mg/kg) also shows significant association, reflecting co-precipitation under reducing conditions. Among trace metals, Zn (22.101–37.022 mg/kg) and Cu (12.503–22.129 mg/kg) show moderate enrichment, consistent with their known affinity for sulfide mineral formation. Pb (11.016–25.791 mg/kg) is also appreciable, while Cd remains low (0.312–1.147 mg/kg), reflecting its weaker sulfide stability (Turekian & Wedepohl (1961).

Ni, Co, and Cr occur at moderate levels, suggesting partial incorporation into resistant mineral phases. The statistical summary **Table 8b** confirms the dominance order: Fe > Mn > Zn > Cu > Pb > Ni > Co > Cr > Cd, indicating strong geochemical stabilization of Fe and Mn in this fraction (Adriano, (2001).

Spatially, higher values in SQ3, SQ4, and SQ15 suggest localized reducing conditions or sulfide enrichment, while lower values in SQ6 and SQ10 indicate weaker sulfide association. **Figure 9** shows the same pattern, with Fe and Mn dominating across all samples. Overall, this phase represents a stable metal reservoir with low immediate mobility, though it may become a secondary source of metals under oxidative environmental changes (Davidson et al., 1994).

Table 8a: Heavy metal concentrations in the sulfide/strongly bound phase (mg/kg). The table shows metals strongly associated with sulfide minerals and resistant phases, reflecting their low mobility and long-term geochemical stability within the soil matrix.

Samples	Fe	Mn	Pb	Cu	Zn	Ni	Co	Cr	Cd
	(mg/Kg)	(mg/Kg)	(mg/Kg)	(mg/Kg)	(mg/Kg)	(mg/Kg)	(mg/Kg)	(mg/Kg)	(mg/Kg)
SQ 1	251.118	105.746	18.723	14.103	31.411	11.652	6.342	5.126	0.343
SQ 2	252.049	108.224	17.916	14.321	30.782	11.761	6.226	5.472	0.345
SQ 3	345.371	147.602	24.432	20.438	35.255	15.004	7.752	6.159	0.798
SQ 4	352.217	147.916	25.543	20.825	36.126	15.243	8.116	6.458	1.128
SQ 6	184.382	83.239	12.621	13.127	26.134	9.827	4.279	4.174	0.312
SQ7	186.641	84.043	12.584	13.312	26.187	10.022	4.853	4.956	0.331
SQ 8	262.248	115.741	19.251	14.329	31.732	12.021	6.349	5.765	0.372
SQ 10	201.508	75.148	11.016	12.503	22.101	8.217	4.251	4.329	0.314
SQ 11	205.421	77.713	11.172	13.008	23.061	8.734	4.584	4.457	0.325
SQ 12	216.142	85.062	11.729	13.543	27.658	10.964	5.866	4.586	0.337
SQ 13	217.618	84.927	11.972	13.729	27.851	11.492	5.982	8.148	0.421
SQ 14	250.354	106.109	18.649	15.021	30.496	12.035	6.264	5.228	0.432
SQ 15	353.506	150.084	25.791	22.129	37.022	15.232	8.335	6.784	1.147
SQ 16	253.127	107.732	18.069	16.011	32.029	12.022	6.016	5.822	0.441
SQ 17	184.783	85.106	11.967	12.938	25.867	10.112	5.241	5.013	0.437

Table 8b: Statistical summary of the heavy metals concentration in the sulfide/strongly bound phase (mg/kg). This table presents the minimum, maximum, and mean concentrations of metals strongly bound within sulfide and resistant mineral phases, indicating their low mobility and high geochemical stability.

Metal	Fe	Mn	Pb	Cu	Zn	Ni	Co	Cr	Cd
Min	184.382	75.148	11.016	12.503	22.101	8.217	4.251	4.174	0.312
Max	353.506	150.084	25.791	22.129	37.022	15.243	8.335	8.148	1.147
Mean	247.766	104.293	16.762	15.289	29.581	11.623	6.030	5.498	0.499

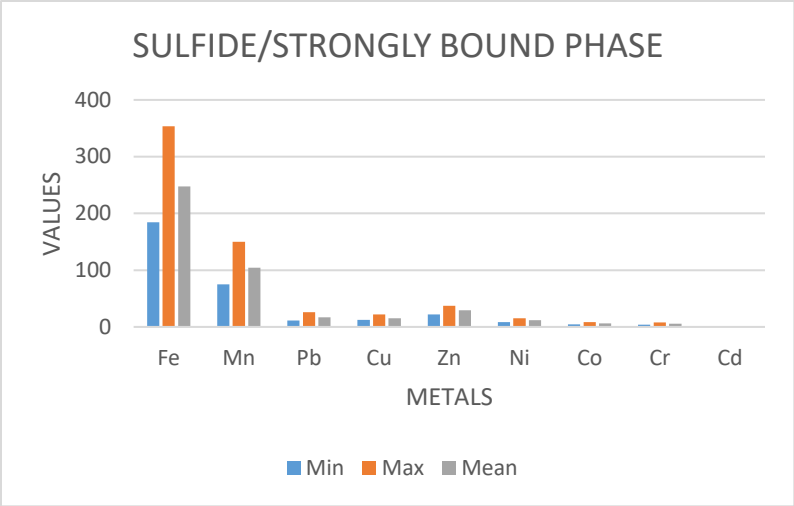

Figure 9. Cluster column chart of the heavy metal concentrations in the sulfide/strongly bound phase (mg/kg). The figure illustrates the distribution of metals strongly bound to sulfide and resistant mineral phases across all samples, highlighting their relative stability and low mobility in the geochemical system.

4.7 The residual phase

The residual phase represents metals strongly incorporated within primary and secondary mineral lattices (e.g., silicates, aluminosilicates, and resistant oxides), and it is widely regarded as the most stable and least mobile fraction in sequential extraction studies. Metals in this fraction are generally considered geochemically inert under normal environmental conditions and are only released through prolonged weathering or complete mineral breakdown (Tessier et al., 1979; Kabata-Pendias, 2011).

From **Table 9a**, Fe exhibits extremely high concentrations (12,532.459–16,416.143 mg/kg), confirming its dominance within primary silicate and ferromagnesian mineral structures. Mn (769.814–946.516 mg/kg) also shows strong lithogenic control, reflecting incorporation into silicate lattices and resistant oxide phases. Among trace metals, Zn (65.905–97.151 mg/kg) and Cu (51.031–62.631 mg/kg) occur at moderate levels, indicating structural substitution within aluminosilicate minerals (Adriano, (2001). Pb (30.574–42.028 mg/kg) and Ni (29.364–43.833 mg/kg) similarly reflect lithogenic inheritance rather than secondary enrichment. Co (13.196–23.146 mg/kg) and Cr (55.704–80.015 mg/kg) are relatively elevated in this phase, consistent with their strong affinity for incorporation into mafic and ultramafic mineral structures Birth (2003). Cd remains very low (0.414–1.302 mg/kg), reflecting its limited structural incorporation and geochemical rarity in resistant mineral phases. The statistical summary **Table 9b** confirms the dominance order: **Fe > Mn > Zn > Cr > Cu > Ni > Co > Pb > Cd**, indicating strong lithogenic control and minimal influence of secondary mobilization processes (Adriano, (2001). The narrow variability across samples further supports a uniform bedrock-derived geochemical signature (Hakanson (1980).

Spatially, higher concentrations in SQ3, SQ4, SQ14, and SQ15 reflect zones enriched in ferromagnesian minerals or more mafic lithological influence, while relatively lower values in SQ6, SQ10, and SQ13 suggest more felsic or weathered lithologies. This spatial pattern is consistent with basement complex terrains where elemental distribution is primarily controlled by parent rock composition rather than anthropogenic inputs (Rahaman 1988).

Figure 10 further confirms this interpretation, showing clear dominance of Fe and Mn across all samples, with other trace metals forming subordinate but stable distributions within the residual matrix. This reinforces the conclusion that most metals are

locked within primary mineral structures and are not readily available for environmental mobilization (Müller (1969).

Overall, the residual phase represents a long-term geochemical reservoir with negligible immediate environmental risk. However, it serves as a key indicator of bedrock composition and mineralogical control in the Ikole–Itapaji area, consistent with established sequential extraction frameworks in crystalline basement environments (Kabata-Pendias, 2011; Alloway, 2013).

Table 9a: Heavy metal concentrations in the residual phase (mg/kg). The table shows metals strongly locked within primary and secondary mineral lattices, representing the most stable and least mobile geochemical fraction in the soil system.

Samples	Fe (mg/Kg)	Mn (mg/Kg)	Pb (mg/Kg)	Cu (mg/Kg)	Zn **(mg/Kg)**	Ni (mg/Kg)	Co g/Kg)	Cr (mg/Kg)	Cd (mg/Kg)
SQ 1	13124.153	851.125	37.231	51.609	86.332	31.861	18.715	66.322	0.597
SQ 2	13231.582	862.197	35.793	52.096	84.809	32.168	19.207	66.188	0.553
SQ 3	16265.625	946.516	40.714	62.631	95.119	42.732	23.061	78.751	1.177
SQ 4	16416.143	941.849	42.028	61.979	97.151	43.833	23.146	80.015	1.185
SQ 6	15693.198	874.034	38.624	56.235	93.009	40.635	21.081	72.231	0.682
SQ7	12758.903	780.623	32.627	53.018	66.745	30.561	13.196	57.592	0.414
SQ 8	14753.727	865.106	36.942	54.723	88.126	34.642	20.731	68.685	1.127
SQ 10	12593.684	789.702	30.574	51.052	65.905	29.364	14.211	55.885	0.534
SQ 11	12682.363	776.937	31.077	51.031	68.016	29.902	13.723	55.759	0.511
SQ 12	14723.794	867.369	38.362	56.387	86.972	34.558	20.148	69.101	0.746
SQ 13	12532.459	769.814	30.984	52.125	68.132	32.092	13.741	55.704	0.642
SQ 14	15562.525	876.614	39.072	58.521	90.165	38.965	22.094	73.672	0.779
SQ 15	15469.538	872.607	40.729	57.985	92.007	39.018	21.628	71.961	1.302
SQ 16	13063.523	856.735	35.071	53.081	84.717	35.109	18.591	67.412	0.698
SQ 17	13274.221	842.699	34.866	52.983	85.458	35.238	18.793	66.923	0.602

Table 9b: Statistical summary of heavy metals in the residual phase (mg/kg). This table presents the minimum, maximum, and mean concentrations of metals retained in the residual fraction, representing the most stable and structurally bound geochemical pool in the soil matrix.

Metal	**Fe**	**Mn**	**Pb**	**Cu**	**Zn**	**Ni**	**Co**	**Cr**	**Cd**
Min	12532.459	769.814	30.574	51.031	65.905	29.364	13.196	55.704	0.414
Max	16416.143	946.516	42.028	62.631	97.151	43.833	23.146	80.015	1.302
Mean	14143.029	851.595	36.313	55.030	83.511	35.379	18.804	67.080	0.770

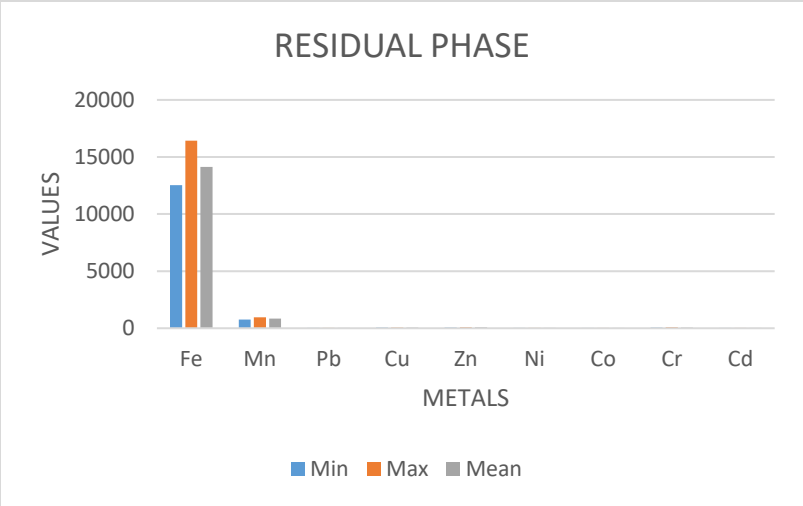

Figure 10. Cluster column chart of the heavy metal concentrations in the residual phase (mg/kg). The figure illustrates the distribution of metals in the residual fraction, highlighting their strong lithogenic control and dominance within primary mineral structures across all samples.

4.8 Ecological Risk Index (ERI)

The Ecological Risk Index Table 10 and the clustered column chart Figure 11 collectively provide a concise understanding of the spatial distribution of heavy metal contamination and associated ecological risk in the Ikole–Itapaji soils. The combined interpretation reveals that variations in ecological risk are strongly controlled by differences in heavy metal enrichment, particularly cadmium (Cd) (Adriano, (2001). .

The clustered column chart indicates that Cd exhibits the most pronounced enrichment relative to other metals across all sampling locations, while Pb shows moderate enrichment at selected sites. In contrast, Mn, Cu, Zn, Ni, Co, and Cr display relatively low and consistent concentrations, suggesting a predominantly lithogenic control associated with the weathering of the underlying Basement Complex rocks. This pattern is consistent with established interpretations of enrichment behavior, where values close to unity indicate natural origins, while elevated values reflect anthropogenic influence (Förstner & Wittmann, 2012; Reimann & de Caritat, 2005).

This enrichment pattern is directly reflected in the Ecological Risk Index results, where SQ4 and SQ15 record the highest ERI values (629.72 and 655.88, respectively), classifying them as very high ecological risk zones. These same locations correspond to peak Cd enrichment in the clustered column chart, confirming cadmium as the primary driver of ecological risk in the study area (Hakanson (1980). The consistency between enrichment behavior and ERI values highlights the strong influence of Cd toxicity in controlling overall ecological risk (Adriano, (2001).

Spatially, contamination is characterized by distinct hotspots rather than a uniform distribution. SQ4 and SQ15 represent major pollution centers, while SQ10 and SQ11 show comparatively low enrichment and lower ERI values, reflecting relatively unimpacted conditions and near-background geochemical signatures (Müller (1969). The selective enrichment of Cd and, to a lesser extent, Pb, suggests localized

anthropogenic inputs such as agricultural activities and waste-related contamination superimposed on a largely natural geochemical environment (Müller, 1969; Tessier et al., 1979).

Overall, the integrated results indicate that while most metals are governed by natural geological processes, Cd—and to a lesser extent Pb—shows clear anthropogenic enrichment, leading to elevated ecological risk at specific locations within the study area. This underscores the need for targeted environmental monitoring in identified hotspots to mitigate potential ecological impacts (Reimann & de Caritat, 2005).

Table 10. Ecological Risk Index (ERI) of heavy metals in soils of the Ikole–Itapaji area, assessing the potential ecological risk posed by individual metals and providing an integrated measure of environmental toxicity across the sampled locations.

Sample	ERI
SQ1	266.52
SQ2	267.72
SQ3	565.49
SQ4	629.72
SQ6	264.76
SQ7	234.35
SQ8	399.79
SQ10	233.17
SQ11	237.51
SQ12	285.37
SQ13	281.75
SQ14	326.64
SQ15	655.88
SQ16	311.92
SQ17	306.23

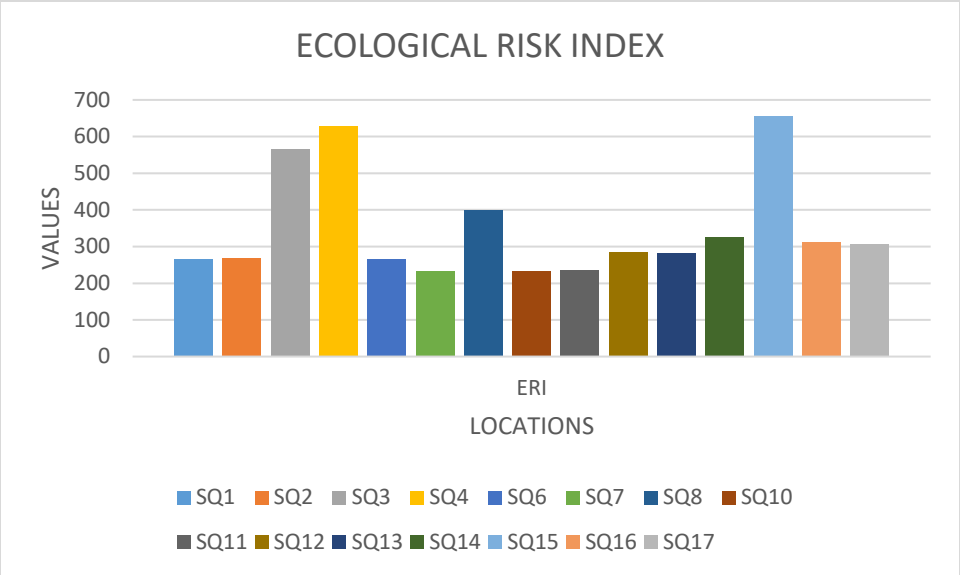

Figure 11. Clustered column chart of heavy metal concentrations showing the ecological risk index (ERI), illustrating the relative contribution of individual metals to overall ecological risk and highlighting spatial variations in contamination intensity across the study area.

4.9 Mobility Factor (MF %)

Table 11 presents the Mobility Factor (MF) values for heavy metals across the 17 sampling locations in the Ikole–Itapaji area, providing insight into the proportion of metals present in the labile and potentially bioavailable fractions of the soil. Overall, the results show relatively low MF values ranging from approximately 2.7% to 4.0%, indicating that most of the heavy metals are predominantly associated with stable, non-labile fractions. This suggests strong geogenic control, consistent with metal stabilization within the Basement Complex lithology, where metals are largely retained in residual and strongly bound phases (Tessier et al., 1979; Reimann & de Caritat, 2005).

Despite this overall stability, subtle spatial variations are observed in Table 11, with SQ4 (3.95%) and SQ15 (3.92%) recording the highest mobility values, while SQ10 and SQ7 exhibit the lowest values (around 2.7–2.8%). These variations indicate localized differences in metal partitioning, with certain sites showing a slightly higher proportion of metals in more reactive and environmentally available forms (Turekian & Wedepohl (1961).

Figure 12 (clustered column chart) visually reinforces this pattern by illustrating the relatively uniform distribution of MF values across all sampling points, with only minor peaks at SQ4 and SQ15. The chart clearly demonstrates that although mobility is generally low across the study area, specific hotspots exhibit marginally elevated metal availability, reflecting localized geochemical disturbance.

When Table 11 and Figure 12 are interpreted together, a consistent spatial pattern emerges. The highest mobility values coincide with the same locations previously identified as contamination hotspots in the ecological risk assessment (SQ4 and SQ15), suggesting that areas of elevated metal loading also tend to exhibit slightly increased metal mobility. Conversely, sites such as SQ10 and SQ7 show both low mobility and comparatively lower contamination levels, indicating relatively stable and less impacted geochemical conditions (Turekian & Wedepohl (1961).

Although the MF values are generally low across the study area, their environmental significance should not be underestimated, particularly for toxic

elements such as cadmium. Even small proportions of bioavailable metals can contribute to plant uptake, soil–water transfer, and long-term ecological exposure due to cadmium's high toxicity and mobility behavior (Tessier et al., 1979; Reimann & de Caritat, 2005).

Overall, the combined interpretation of Table 11 and Figure 12 indicates that the Ikole–Itapaji soils are largely geochemically stable, but with localized zones (notably SQ4 and SQ15) where slightly enhanced mobility corresponds with higher contamination levels (Hakanson (1980). These findings highlight the importance of targeted environmental monitoring in identified hotspot areas to prevent potential long-term ecological impacts.

Table 11. Mobility Factor (MF %) of heavy metals in soils of the Ikole–Itapaji area, expressed as the average percentage mobility across all analyzed metals per sample, indicating the proportion of metals present in readily mobile and environmentally available fractions across the study area.

Sample	MF (%)
SQ1	3.42
SQ2	3.36
SQ3	3.89
SQ4	3.95
SQ6	3.28
SQ7	3.21
SQ8	3.67
SQ10	2.74
SQ11	2.86
SQ12	3.31
SQ13	3.29
SQ14	3.58
SQ15	3.92
SQ16	3.40
SQ17	3.33

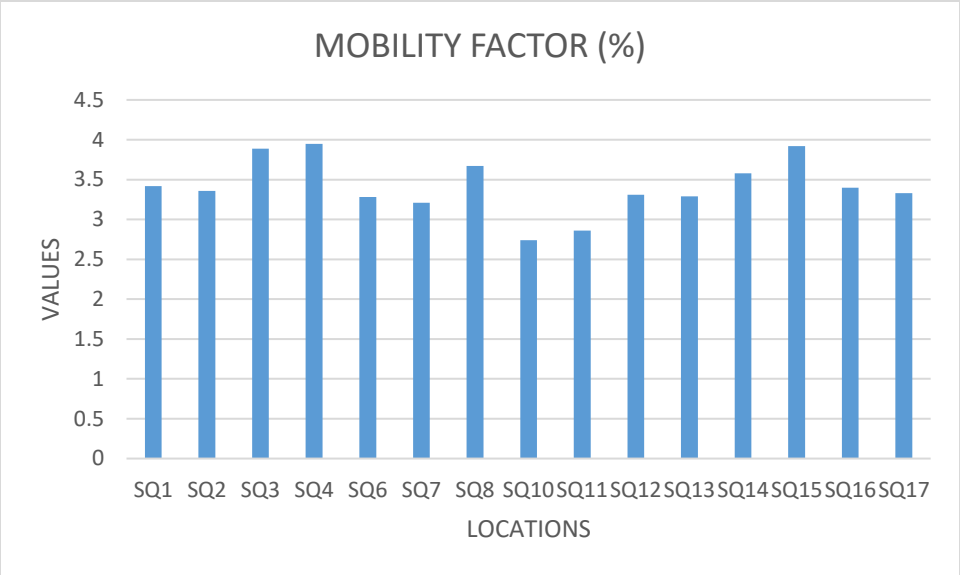

Figure 12. Clustered column chart of heavy metal concentrations showing the mobility factors (MF), illustrating the proportion of each metal present in readily mobile and bioavailable fractions and highlighting spatial variations in metal mobility across the study area.

5.0 CONCLUSION

This study assessed the ecological risk and mobility behavior of selected heavy metals in soils from the Ikole–Itapaji area, Southwestern Nigeria, using the Ecological Risk Index (ERI) and Mobility Factor (MF). The integrated results reveal that heavy metal distribution and environmental behavior in the area are strongly controlled by both natural geochemical processes associated with the Basement Complex lithology and localized anthropogenic influences.

The ERI results indicate that ecological risk is spatially variable, with SQ4 and SQ15 identified as very high-risk hotspots, while most other sampling locations fall within moderate to considerable risk categories. This pattern suggests that ecological risk in the study area is not uniformly distributed but is concentrated in specific locations, largely driven by elevated cadmium contributions, which significantly influence the overall toxicological burden of the soils.

The Mobility Factor results further show that heavy metals in the study area are generally characterized by low mobility, with values ranging from approximately 2.7% to 4.0%. This indicates that most metals are strongly bound to stable soil fractions, reflecting dominant lithogenic control and limited immediate bioavailability. However, slightly higher mobility values at SQ4 and SQ15 suggest localized enhancement of metal reactivity, which corresponds with the same hotspots identified in the ERI assessment.

The combined interpretation of ERI and MF demonstrates a clear relationship between contamination intensity and metal behavior, where areas with higher ecological risk also exhibit relatively increased mobility. Although overall mobility remains low, the presence of even small bioavailable fractions—particularly for highly toxic elements such as cadmium—poses potential long-term environmental concerns, including soil–plant transfer and possible groundwater contamination.

In conclusion, the Ikole–Itapaji soils are generally geochemically stable but exhibit localized zones of significant environmental concern. SQ4 and SQ15 represent critical contamination hotspots that require attention due to their elevated ecological risk and comparatively higher metal mobility. These findings emphasize the need for targeted environmental monitoring and land-use management strategies to mitigate potential ecological and human health risks associated with heavy metal accumulation in the area.

5.1 RECOMMENDATIONS

Based on the findings of this study, the following recommendations are proposed to mitigate potential ecological and environmental risks associated with heavy metal accumulation in the Ikole–Itapaji soils:

1. **Targeted Environmental Monitoring:**
   Continuous monitoring of soil quality should be prioritized at identified hotspots, particularly SQ4 and SQ15, where both Ecological Risk Index (ERI) and Mobility Factor (MF) values indicate elevated contamination and potential metal reactivity.
2. **Soil and Agricultural Management:**
   Farmers within the study area should be sensitized on the risks associated with heavy metal accumulation, especially cadmium. The use of contaminated soils for food crop cultivation in high-risk zones should be discouraged or strictly regulated.
3. **Source Identification and Control:**
   Further investigations should be conducted to identify specific anthropogenic sources contributing to cadmium and lead enrichment, with a view to implementing appropriate control measures such as waste management regulation and reduction of agrochemical inputs.
4. **Environmental Remediation Strategies:**
   In severely impacted locations, remediation approaches such as phytoremediation, soil amendment (e.g., organic matter and biochar application), and stabilization techniques should be considered to reduce metal mobility and ecological risk.
5. **Policy and Land-Use Planning:**
   Local environmental and land-use authorities should incorporate geochemical risk maps into planning frameworks to prevent sensitive land use (e.g., agriculture and residential development) in high-risk zones.

5.2 LIMITATIONS OF THE STUDY

This study is subject to certain limitations that should be considered when interpreting the results:

1. **Spatial Sampling Density:**
   Although 17 sampling locations provide useful spatial coverage, a higher sampling density could improve the resolution of contamination hotspot mapping and better capture micro-scale variability.
2. **Temporal Limitation:**
   The study represents a single sampling period; therefore, seasonal variations in metal mobility and ecological risk were not assessed. Temporal changes due to rainfall and land-use activities may influence metal behavior.
3. **Restricted Contaminant Scope:**
   The study focused only on selected heavy metals. Other potentially relevant contaminants such as hydrocarbons or emerging pollutants were not considered.
4. **Absence of Direct Biological Assessment:**
   Ecological risk was evaluated using ERI and MF models without direct biological indicators (e.g., plant uptake or microbial response), which could have provided additional validation of ecological impacts.
5. **Source Apportionment Constraints:**
   While the results suggest both lithogenic and anthropogenic influences, the study did not include advanced source apportionment techniques (e.g., isotopic tracing or receptor modeling) to quantify contributions precisely.

Availability of Data and Materials

The datasets used and analyzed during this study are available from the corresponding author upon reasonable request.

Disclaimer (Artificial Intelligence)

During the preparation of this work, the authors used ChatGPT (GPT-5-mini) to assist with language editing and content organization. After using this tool, the authors reviewed, revised, and verified all content to ensure accuracy, originality, and authenticity, and take full responsibility for the

content of the published article.

Competing Interests

The authors have declared that no competing interests exist.

Authors' Contributions

Adeleke Ojo contributed to the conceptualization and design of the study, field sampling, laboratory analysis, data interpretation, and preparation of the initial manuscript draft. **Olusola Amos Olaolorun** was involved in supervising the research work, conducting the methodological review, interpreting geochemical results, and critically revising the manuscript for important intellectual content. **Adeyinka Aturamu** contributed to data processing, statistical and geochemical analysis, literature review, and editing of the final manuscript. All authors read and approved the final version of the manuscript.

REFERENCES

1. Abule, E. C., & Ekpete, O. A. (2025). Geochemical speciation and environmental implications of heavy metal mobility. https://doi.org/10.63561/fnas-jsi.v6i3.955
2. Adetunla, F. R., Ayodele, O. S., Asowata, I. T., & Olususi, J. (2025). Integrated geological, aeromagnetic and remote sensing datasets in litho-structural mapping of basement rocks in southwestern Nigeria. *Asian Journal of Geological Research, 8*(3), 523–553. https://doi.org/10.9734/ajoger/2025/v8i3213
3. Adriano, D. C. (2001). *Trace Elements in Terrestrial Environments: Biogeochemistry, Bioavailability, and Risks of Metals*. Springer, New York. https://link.springer.com/book/10.1007/978-0-387-21510-5
4. Alloway, B. J. (2013). *Heavy Metals in Soils: Trace Metals and Metalloids in Soils and Their Bioavailability* (3rd ed.). Springer. https://doi.org/10.1007/978-94-007-4470-7
5. Birth, G. (2003). A scheme for assessing human impacts on coastal aquatic environments using sediments. https://doi.org/10.1007/978-3-662-05950-8_7
6. Bouazizi, N., Baraud, F., Lemoine, M., & Leleyter, L. (2023). Shortened sequential extraction procedure: An effective and time-saving determination of trace metals in sediments. *Soil and Sediment Contamination*. https://doi.org/10.1080/15320383.2023.2293879
7. Çelebi, E. E. (2024). Determination of metal fractions and rare earth anomalies using modified sequential extraction. *Environmental Earth Sciences, 83*, 93. https://doi.org/10.1007/s12665-023-11409-w
8. Davidson, C. M., Duncan, A. L., Littlejohn, D., Ure, A. M., & Garden, L. M. (1998). A critical evaluation of the three-stage BCR sequential extraction procedure to assess the potential mobility and toxicity of heavy metals in industrially contaminated land. *Analytica Chimica Acta, 363*(1–2), 45–55. https://doi.org/10.1016/S0003-2670(98)00057-9
9. De Matteis, C., Mantovani, L., Tribaudino, M., et al. (2023). Sequential extraction procedure of municipal solid waste incineration bottom ash targeting grain size and amorphous fraction. *Frontiers in Environmental Science, 11*, 1254205. https://doi.org/10.3389/fenvs.2023.1254205
10. Delina, R. E. G. (2024). Partitioning and mobility of chromium using sequential extraction. *Environmental Science & Technology*. https://doi.org/10.1021/acs.est.3c10774
11. Doi, T., Hamasaki, S., Yamamoto, H., et al. (2023). Dynamic sequential extraction procedure for extracting mercury from soil samples. *Analytical Sciences, 39*(5), 739–748. https://doi.org/10.1007/s44211-023-00313-9

12. Filgueiras, A. V., Lavilla, I., & Bendicho, C. (2002). Chemical sequential extraction for metal partitioning in environmental solid samples. *Journal of Environmental Monitoring, 4*, 823–857. https://doi.org/10.1039/B207574C
13. Firmino, F. H. T., et al. (2025). Efficiency of sequential extraction schemes in partitioning toxic elements. *European Journal of Soil Science*. https://doi.org/10.1111/ejss.70090
14. Förstner, U., & Wittmann, G. T. W. (2012). *Metal Pollution in the Aquatic Environment*. Springer. https://doi.org/10.1007/978-3-642-69385-4
15. Hakanson, L. (1980). An ecological risk index for aquatic pollution control: A sedimentological approach. *Water Research, 14*(8), 975–1001. https://doi.org/10.1016/0043-1354(80)90143-8
16. Ibrahim, R., et al. (2024). Sequential extraction of heavy metals in soils. https://doi.org/10.33003/fjs-2024-0803-2451
17. Kabata-Pendias, A. (2011). *Trace Elements in Soils and Plants* (4th ed.). CRC Press. https://doi.org/10.1201/b10158
18. Kaiser, K., & Kalbitz, K. (2012). Cycling downwards – dissolved organic matter in soils. *Soil Biology and Biochemistry, 52*, 29–32. https://doi.org/10.1016/j.soilbio.2012.04.002
19. Liu, J., et al. (2022). Speciation of heavy metals in soils and their immobilization at micro-scale interfaces among soil components. *Science of the Total Environment, 825*, 153862. https://doi.org/10.1016/j.scitotenv.2022.153862
20. Müller, G. (1969). Index of geoaccumulation in sediments of the Rhine River. *GeoJournal, 2*(3), 108–118. https://www.semanticscholar.org/paper/INDEX-OF-GEOACCUMULATION-IN-SEDIMENTS-OF-THE-RHINE-Muller/03688e2c0b4cabea9023db05e6b9a33281f0ea06
21. Nigerian Geological Survey Agency (NGSA). (2006). *Geophysical Mapping of Nigeria: Airborne Radiometric and Magnetic Survey Data, 2006*. Available at: https://ngsa.gov.ng
22. Ogah, A. J., & Abubakar, F. (2024). Solid mineral potential evaluation using integrated aeromagnetic and aeroradiometric datasets. *Scientific Reports, 14*, 1637. https://doi.org/10.1038/s41598-024-52270-6
23. Ojo, O. F., Osazuwa, B. I., Chiemeke, C. C., Osumeje, O. J., Oyedele, A. A., Adagunodo, T. A., Oyeyemi, K. D., & Ejiga, E. G. (2024). Classification of the basement complex using aeromagnetic and remote sensing data analyses: Case study of Ekiti State, southwestern Nigeria. *Earth Sciences Malaysia, 8*(2), 158–162. https://doi.org/10.26480/esmy.02.2024.158.162
24. Oyinloye, A. O. (2011). Geology and geotectonic setting of the basement complex rocks in Southwestern Nigeria: Implications on provenance and evolution. https://doi.org/10.5772/26990
25. Rahaman, M. A. (1988). Recent Advances in the Study of the Basement Complex of Nigeria. In *Precambrian Geology of Nigeria* (pp. 11–41). Geological Survey of Nigeria, Kaduna. https://www.scirp.org/reference/referencespapers?referenceid=1712445
26. Reimann, C., & de Caritat, P. (2005). Distinguishing between natural and anthropogenic sources for elements in the environment. *Science of the Total Environment, 337*, 91–107. https://doi.org/10.1016/j.scitotenv.2004.06.011
27. Reimann, C., & de Caritat, P. (2012). *Chemical Elements in the Environment: Factsheets for the Geochemist and Environmental Scientist*. Springer. https://doi.org/10.1007/978-3-642-72016-1
28. Salako, K. A., Adetona, A. A., Rafiu, A. A., Augie, A. I., Jimoh, M. O., Alkali, A., Muriana, R. A., & Lawrence, J. O. (2024). Integrated geophysical investigation for gold mineralization potential over the southern parts of Kebbi State, northwestern Nigeria.

Heliyon, *10*(14), e34093. https://doi.org/10.1016/j.heliyon.2024.e34093

29. Souza, J. P. R., Garnier, J., Quintarelli, J. M., et al. (2024). Adapted sequential extraction protocol for mercury speciation in mining environments. *Toxics*, *12*(5), 326. https://doi.org/10.3390/toxics12050326
30. Tessier, A., Campbell, P. G. C., & Bisson, M. (1979). Sequential extraction procedure for the speciation of particulate trace metals. *Analytical Chemistry*, *51*, 844–851. https://doi.org/10.1021/ac50043a017
31. Turekian, K. K., & Wedepohl, K. H. (1961). Distribution of the elements in some major units of the Earth's crust. *Geological Society of America Bulletin*, *72*(2), 175–192. https://doi.org/10.1130/0016-7606(1961)72[175:DOTEIS]2.0.CO;2
32. Wei, B., & Yang, L. (2010). A review of heavy metal contaminations in urban soils, urban road dusts and agricultural soils from China. *Microchemical Journal*, *94*(2), 99–107. https://doi.org/10.1016/j.microc.2009.09.014